

A robust autoassociative memory with coupled networks of Kuramoto-type oscillators

Daniel Heger and Katharina Krischer*
Physics Department, Technical University of Munich,
85748 Garching, James-Franck-Str. 1, Germany

Uncertain recognition success, unfavorable scaling of connection complexity or dependence on complex external input impair the usefulness of current oscillatory neural networks for pattern recognition or restrict technical realizations to small networks. We propose a new network architecture of coupled oscillators for pattern recognition which shows none of the mentioned flaws. Furthermore we illustrate the recognition process with simulation results and analyze the new dynamics analytically: Possible output patterns are isolated attractors of the system. Additionally, simple criteria for recognition success are derived from a lower bound on the basins of attraction.

I. INTRODUCTION

Synchronization of oscillators, i.e., "the adjustment of rhythms due to an interaction" [1], is a ubiquitous concept leading to collective dynamics. Its occurrence spreads over all scientific disciplines, with applications in engineering, physics, chemistry, biology, medicine and even in social sciences. The study of synchronization behavior has been correspondingly intense during the last two to three decades, the state of the art being summarized in recent textbooks, monographs and focus issues [1–8].

A particularly intriguing area where synchronization often occurs is neuroscience. The synchronization of neural oscillators controls vital functions but is responsible for neural diseases as well. Synchronization phenomena are also involved in cognition tasks of the brain [9]. The wish to understand and mimic information processing of the brain led to a separate field called computational neuroscience. Concomitantly, novel types of hardware were proposed that mimic some aspects of neural information processing. Their massively parallel operation is inherently different from the operating modes of all types of processors in everyday hardware. In this manuscript, we discuss a novel coupling scheme for oscillators that generates synchronization patterns and thus can be used as an autoassociative memory.

When an *autoassociative memory* is presented with a defective and/or incomplete piece of data, it recognizes and retrieves the correct data from a set of correct candidates. From a different point of view, the defective input data are mapped onto the most similar of the candidates. The ability to "map" is also found in complex physical systems: The trajectory of a system state will converge to an attractor. If several attractors exist, different sets of initial conditions, called *basins of attraction*, will end up on different attractors. Therefore, the system "maps" all initial conditions within one basin onto its attractor. Note that few physical systems are actually suitable as autoassociative memories: First, suitable mappings of the defective data onto the initial conditions and from

the attractors back onto the correct patterns have to be found. Additionally, initial conditions as well as attractors of a system need to be controlled, with the latter usually being difficult. Finally, the initial defective data should be mapped onto the most similar correct data candidate, which requires that the basins of attraction actually conform with a sensible definition of similarity. Also note that the idea to use basins of attractions for pattern recognition has originally been proposed by Hopfield for use in neural networks [10]. Contributions from mathematics, physics and neuroscience (see the end of [11] for a summary) made it possible to merge his ideas with the studies of coupled nonlinear oscillators.

Networks of nonlinear oscillators have been shown to act as autoassociative memory devices for binary patterns [12–19] according to the above-mentioned principle. In the first architecture [12–14], identical Kuramoto oscillators [11] are fully interconnected via programmable connections that can change sign and strength of the coupling according to the Hebbian Rule [20]. If the dynamics are expressed in phase shifts, fixed points are the only type of attractors, and defective input patterns as well as correct pattern candidates can be mapped on two synchronized groups of oscillators whose phases differ by π .

However, this design has two disadvantages:

- No distinct, well-separated fixed points exist for the memorized patterns [21]. Instead, there is one global attractor consisting of lines of attractive fixed points with neutrally stable eigendirections that connect every memorized pattern with every other. On short timescales, pattern recognition still works: Starting at the defective pattern, the system state quickly relaxes onto the global attractor close to the most similar pattern. On the attractor, however, perturbations due to external noise or implementation inaccuracies dominate and the system state drifts away from the correct pattern on longer timescales. Additionally, recognition success cannot be guaranteed as no well-defined basin of attraction exists for any single output pattern.
- The number of connections scales quadratically with the number of oscillators, so no large networks can be implemented in hardware.

* Contact: daniel.heger@ph.tum.de and krischer@ph.tum.de

So far, no architecture that solves both issues has been proposed. However, separate solutions for each problem have been discussed: Nishikawa et al. [18] showed that the degeneracy of the attractor can be lifted by adding second order Fourier modes to the coupling. A similar network with third order Fourier modes has been proposed as well [19]. A partial solution for the scaling problem has been proposed by Hoppensteadt and Izhikevich [15] and has been further advanced by Hölzel and Krischer [16] and Kostorz et al. [17]: Oscillators of different frequencies are coupled to the same global coupling that affects every oscillator differently. These architectures require an external input of complex time-dependent functions, but the number of connections scales with $\mathcal{O}(N)$.

Our architecture combines isolated attractors and minimal scaling of connection complexity without the need for complex external input. To this end, we built on previous studies [15, 16] of globally coupled oscillatory devices, but we introduce two peculiar features: Different temporal modulation of the coupling strength and a replacement of the single network by two interconnected subnetworks. The result is a robust autoassociative memory that is straightforward to be implemented as hardware and can be readily read out. Additionally, we can predict recognition success analytically. Thus, by exploiting the mutual interaction of two sub-networks, we arrive at a network architecture with superior functionality.

In the next section, the structure of our new architecture is described in detail. Afterwards, we obtain the effective dynamics through averaging and analyze its fixed points in Sec. III. In order to predict recognition success, Sec. IV derives a lower bound on the basins of attraction. The resulting criterion for guaranteed matching is then validated with simulations of the full dynamics in Sec. V. Before results are summarized in Sec. VII, Sec. VI compares the architecture to previous autoassociative networks of oscillators.

II. A NEW SCALABLE ARCHITECTURE

Our architecture consists of two identical networks of N oscillators each with equal frequency distribution. Oscillators within each of these "subnetworks" are globally coupled and the coupling strength is additionally modulated in time. For the first network, the coupling modulation[22] is constructed from products of signals of the second network's oscillators and vice versa. Due to its symmetrical layout, which is visualized in Fig. 1, we name the network the MONACO-Architecture: *Mirrored Oscillator Networks for Autoassociative COmputation*.

Motivated by experiments with networks of electrical Van-der-Pol-oscillators [16, 17], we assume that the oscillators are weakly coupled in one variable, have sinusoidal signals and a phase response curve proportional to a cosine. Then, the dynamics can be reduced to a phase

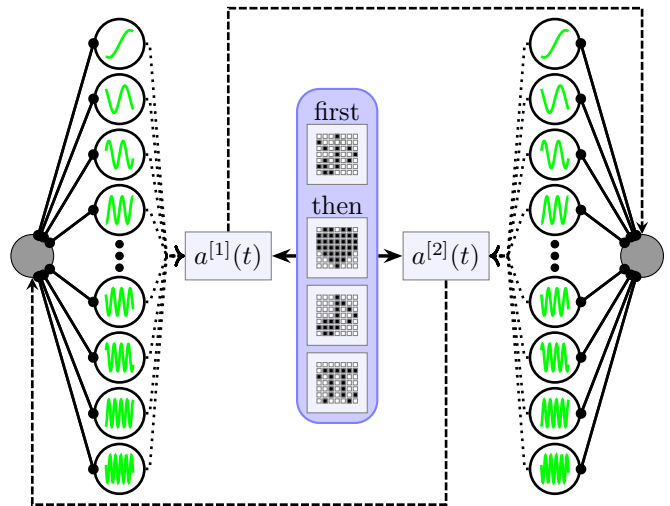


FIG. 1. Schematics of our new MONACO-Architecture: Oscillators (depicted as black circles surrounding a green sine-wave) are divided into two networks with the same frequency distribution that are both globally coupled. Coupling strength of both global couplings is modulated in time with functions $a^{[1]}(t) / a^{[2]}(t)$ that depend on physical signals of oscillators from the other network and patterns shown in the middle.

description [23]:

$$\begin{aligned}
 \dot{\vartheta}_i^{[1]} &= \Omega_i + \cos \vartheta_i^{[1]} \cdot a^{[2]}(t) \cdot \frac{\epsilon}{N} \sum_{j=1}^N \sin \vartheta_j^{[1]} \\
 \dot{\vartheta}_i^{[2]} &= \Omega_i + \cos \vartheta_i^{[2]} \cdot a^{[1]}(t) \cdot \frac{\epsilon}{N} \sum_{j=1}^N \sin \vartheta_j^{[2]} \\
 a^{[1]}(t) &= \sum_{k,l=1}^N S_{kl} \sin \vartheta_k^{[1]} \sin \vartheta_l^{[1]} \\
 a^{[2]}(t) &= \sum_{k,l=1}^N S_{kl} \sin \vartheta_k^{[2]} \sin \vartheta_l^{[2]}
 \end{aligned} \tag{1}$$

$\vartheta_i^{[1]}$ is the phase of the i -th oscillator in the first network and Ω_i its natural frequency. In the global signal $a^{[2]}(t) \cdot \epsilon/N \cdot \sum_{j=1}^N \sin \vartheta_j^{[1]}$, $a^{[2]}(t)$ denotes the coupling modulation generated from the second network's signals and ϵ is a small parameter which will be shown to be the effective coupling strength of the averaged dynamics. The amplitude perturbation is converted into a change in phase by multiplying with the phase response function $\cos \vartheta_i^{[1]}$ and the coupling matrix \mathbf{S} controls attractors of the system.

Note that the frequency distribution is the same in both networks, so N pairs of oscillators with equal frequency exist. For sufficiently weak coupling and specifically chosen frequencies, S_{ij} only effectively connects oscillator pairs i and j and the architecture can act as an autoassociative memory: Apart from $\Omega_i \neq \Omega_j \forall i \neq j$, all frequencies Ω_i must be larger than $\Omega_{max}/3$ and all

difference frequencies $\Delta\Omega_{ij} = \Omega_i - \Omega_j$ must be pairwise different as shown in Appendix A. As we demonstrate below (Eq. (4)), these conditions allow for further simplification of Eq. 1.

As the oscillator pairs of equal frequency synchronize at phase differences $\Delta\vartheta_i = \vartheta_i^{[1]} - \vartheta_i^{[2]}$ of either 0 or π ($\pm 2\pi n$) in this setup, the $\Delta\vartheta_i$ are easy to read out (e.g. with one signal multiplication and a low-pass filter) and will be our "system state" to be manipulated. The coupling matrix is chosen according to the Hebbian Rule [20]:

$$S_{ij} = \sum_{m=1}^M \alpha_i^m \alpha_j^m \text{ with } \alpha_i \in \{\pm 1\} \quad (2)$$

Then attractors will exist for for each pattern $\vec{\alpha}^m$ and its inverse $-\vec{\alpha}^m$ according to the following $\{\Delta\vec{\vartheta} \mapsto \vec{\alpha}\}$ -mapping (see also Sec. III):

$$\begin{aligned} 0 + 2\pi n &\mapsto +1 \\ \pi + 2\pi n &\mapsto -1 \end{aligned} \quad (3)$$

When we talk about patterns "being attractive", it is meant in the sense that attractors in $\Delta\vec{\vartheta}$ exist according to this mapping.

As in [15–17], pattern recognition consists of two steps: During the "initialization" step, the coupling matrix is chosen as $S_{ij} = \alpha_i^d \alpha_j^d$ with a "defective" pattern $\vec{\alpha}^d$. $\vec{\alpha}^d$ is similar to one pattern $\vec{\alpha}^{m'}$ out of M correct patterns $\vec{\alpha}^m$. After the system state moved onto an attractor corresponding to $\vec{\alpha}^d$, the coupling matrix is changed to $S_{ij} = \sum_{m=1}^M \alpha_i^m \alpha_j^m$ at the beginning of the "recognition" step. As the defective pattern is close to the correct pattern $\vec{\alpha}^{m'}$ in phase space, the system state will move to an attractor representing $\vec{\alpha}^{m'}$ and can be read out.

Phase differences $\Delta\vartheta_j$ from an exemplary simulation of the phase dynamics (Eq. (1)) are shown in Fig. 3 for $N = 49$ oscillator pairs. The memorized patterns $\vec{\alpha}^m$ used are visualized in Fig. 2 and are not orthogonal in the sense that $\langle \vec{\alpha}^{m_1}, \vec{\alpha}^{m_2} \rangle \neq 0 \forall m_1, m_2$ and $m_1 \neq m_2$ (\langle, \rangle denotes the standard scalar product.). After initializing a defective pattern $\vec{\alpha}^d$ with 6 erroneous pixels, the coupling matrix is changed to $S_{ij} = \sum_{m=1}^M \alpha_i^m \alpha_j^m$ and the erroneous phase differences change to represent the correct ♣-shaped output pattern in the recognition step.

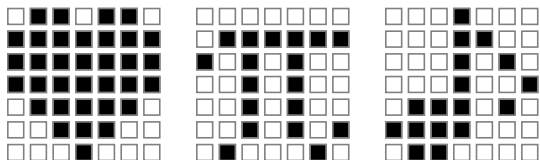


FIG. 2. Nonorthogonal patterns with 49 pixels that were used as memorized patterns $\vec{\alpha}^m$ in simulations for Fig. 3, Fig. 4 and the statistics in Sec. IV. $\alpha_i^m = +1$ is visualized as a white pixel and black pixels correspond to $\alpha_i^m = -1$.

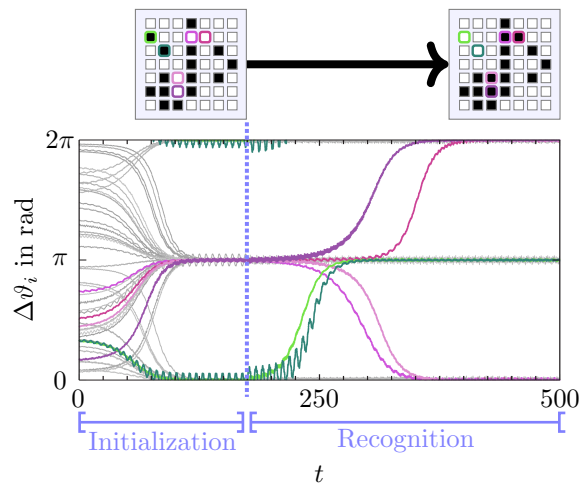


FIG. 3. Successful Recognition Process: A binary pattern with 6 erroneous pixels (colored and thick) shown on the top left is correctly recognized as one of 3 memorized patterns shown in Fig. 2. White pixels are mapped onto $\Delta\vartheta_i = \pi$ and black pixels correspond to $\Delta\vartheta_i = 0$ or 2π . Green trajectories correspond to pixels that are erroneously black, so they should change from $\Delta\vartheta_i = 0$ (or 2π) to $\Delta\vartheta_i = \pi$ in the recognition step, which they do successfully. Similarly, pink trajectories correctly change from π to 0 (or 2π) while gray trajectories, corresponding to already correct pixels, do not change. For simulation details, see Sec. V.

However, the recognition process can fail if the number of erroneous pixels is too large. A failed recognition step is shown in Fig. 4: The system state moves to an unknown attractor which corresponds to none of the $\vec{\alpha}^m$. In order to predict recognition success, a simple criterion is derived and tested in Sec. IV.

Before analyzing the dynamics, we want to point out important details of the architecture design:

- The coupling matrix \mathbf{S} does not need to be wired explicitly, which would require $\mathcal{O}(N^2)$ connections. By rewriting both coupling modulations as squares of scalar products, they can be generated with $\mathcal{O}(N \cdot M)$ connections only:

$$\begin{aligned} a^{[1/2]}(t) &= \sum_{k,l=1}^N \sum_{m=1}^M \alpha_k^m \alpha_l^m \sin \Delta\vartheta_k^{[1/2]} \sin \Delta\vartheta_l^{[1/2]} \\ &= \sum_{m=1}^M \left(\sum_{j=1}^N \alpha_j^m \sin \Delta\vartheta_j^{[1/2]} \right)^2 \end{aligned}$$

Depending on usage, the $\vec{\alpha}^m$ can be hardwired or changed for each recognition process.

- A design with two subnetworks is not necessary in order to obtain isolated attractors, as these are due to our multiplicative coupling modulation and isolated attractors would exist with the following

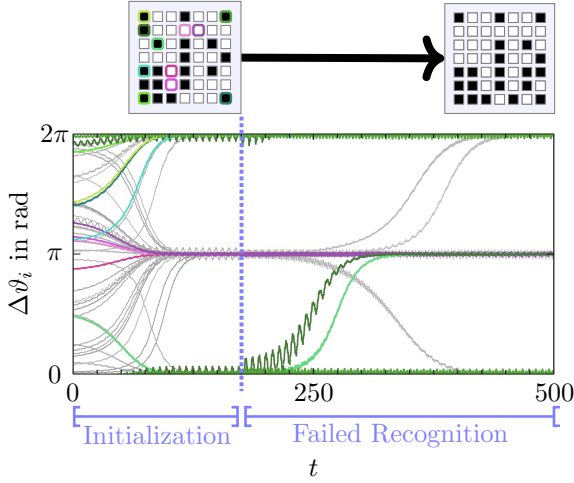


FIG. 4. Recognition process fails due to too many defects: A binary pattern with 11 erroneous pixels (colored) shown on the top left should be recognized as one of 3 memorized patterns shown in Fig. 2. However, the recognition fails: Pink trajectories corresponding to pixels that are erroneously white should change from $\Delta\vartheta_i = \pi$ to $\Delta\vartheta_i = 0$ (or 2π) during the recognition process, but do not. Likewise, only 2 green trajectories change from 0 (or 2π) to $\Delta\vartheta_i = \pi$, although all 7 represent black pixels that should change to white. Additionally 3 gray trajectories, whose corresponding pixels are already correct, change to wrong values. The system settles at the pattern shown on the top right, which is none of the memorized patterns. For simulation details, see Sec. V.

single-network-system:

$$\dot{\vartheta}_i^{[1]} = \Omega_i + \cos \vartheta_i^{[1]} \cdot a_{ext}(t) \cdot \frac{\epsilon}{N} \sum_{j=1}^N \sin \vartheta_j^{[1]}$$

$$a_{ext}(t) = \sum_{k,l=1}^N S_{kl} \sin \Omega_k t \sin \Omega_l t$$

As no oscillators with equal frequencies exist in this setup, however, phase differences are no useful coordinate and phase shifts $\varphi_i = \vartheta_i - \Omega_i t$ must be used instead. Tracking changes of the φ_i requires very precise frequency and time measurements, which renders readout difficult and error-prone. In contrast, binary values of phase differences can easily be read out in the MONACO-architecture by multiplying signals of an oscillator pair and using a low-pass filter, gaining $\cos \Delta\vartheta_i$. Additionally, the effective average coupling strength ϵ is doubled with two subnetworks, enabling faster recognition. (compare with Appendix A)

Another reason is much more subtle: In all architectures with externally generated coupling modulations, frequencies in the coupling modulation are fixed to the natural frequencies of the uncoupled oscillators. However, oscillators change their frequency if coupled due to the so-called "accelera-

tion effect" [24]. We assume this might lead to mismatches between oscillator frequency and coupling modulation frequency components which in turn would further limit the coupling strength ϵ . As a higher coupling strength reduces recognition time, we decided to avoid the problem altogether: Since oscillators in both networks are affected symmetrically by the coupling, the acceleration effect will be equal and frequencies in the coupling modulations are adjusted automatically.

- Attractors exist for every pattern's inverse in addition to the pattern itself (see Sec. III). Therefore, the system state can move to the inverse of the defective pattern $\vec{\alpha}^d$ in the initialization step, which yields the inverse of the correct pattern in the recognition step. If this ambiguity needs to be removed, we suggest to add an equal "parity bit" to all patterns which signals if the output pattern needs to be inverted automatically.
- The MONACO-architecture is a neural network: An oscillator pair corresponds to an artificial neuron that "stores" its phase difference $\Delta\vartheta_i$. The synchronization process can be seen as continuous updating of the $\Delta\vartheta_i$.

III. ANALYSIS OF THE DYNAMICS

A. Simplification of the evolution equations

Prior to determining attractors, we simplify the phase equations (Eq. (1)) with the technique of averaging [25]:

The right hand sides of Eq. (1) consist of many different frequency components. If the coupling strength ϵ is sufficiently small, larger frequencies average out on times much smaller than the largest timescale and the smallest frequencies dominate the dynamics:

$$\begin{aligned} \dot{\vartheta}_i^{[1]} &\approx \Omega_i + \frac{\epsilon M}{8N} \sin(2\Delta\vartheta_i) \\ &\quad - \frac{\epsilon}{4N} \sum_{j=1}^N S_{ij} [\sin(\Delta\vartheta_i + \Delta\vartheta_j) + \sin(\Delta\vartheta_i - \Delta\vartheta_j)] \\ \dot{\vartheta}_i^{[2]} &\approx \Omega_i - \frac{\epsilon M}{8N} \sin(2\Delta\vartheta_i) \\ &\quad + \frac{\epsilon}{4N} \sum_{j=1}^N S_{ij} [\sin(\Delta\vartheta_i + \Delta\vartheta_j) + \sin(\Delta\vartheta_i - \Delta\vartheta_j)] \end{aligned}$$

The lengthy averaging calculation is shown in Appendix A and includes restrictions on the frequency distribution of the oscillators. Using a trigonometric theorem, we can express our equation system with the phase differences $\Delta\vartheta_i$ only:

$$\Delta\dot{\vartheta}_i = \dot{\vartheta}_i^{[1]} - \dot{\vartheta}_i^{[2]} \approx$$

$$\begin{aligned}
& -\frac{\epsilon}{2N} \sum_{j=1}^N S_{ij} [\sin(\Delta\vartheta_i + \Delta\vartheta_j) + \sin(\Delta\vartheta_i - \Delta\vartheta_j)] \\
& + \frac{\epsilon M}{4N} \sin(2\Delta\vartheta_i) \\
\Delta\dot{\vartheta}_i = & -\frac{\epsilon}{N} \sin\Delta\vartheta_i \left(\sum_{j=1}^N S_{ij} \cos\Delta\vartheta_j - \frac{M}{2} \cos\Delta\vartheta_i \right) \quad (4)
\end{aligned}$$

This is the main evolution equation that governs the dynamics of the architecture.

B. Fixed points and their stability

At fixed points $\Delta\vec{\vartheta}^*$ of the dynamics, all velocity components $\Delta\dot{\vartheta}_i$ must vanish. Depending on which factor in Eq. (4) vanishes, pixel indices can be sorted into 2 sets p and q :

$$\begin{aligned}
\bullet \quad i \in p & \Leftrightarrow \sin\Delta\vartheta_i^* = 0 \Leftrightarrow \Delta\vartheta_i^* \in \{0, \pi\} + 2\pi n \\
\bullet \quad i \in q & \Leftrightarrow \sum_{j=1}^N S_{ij} \cos\Delta\vartheta_j^* - \frac{M}{2} \cos\Delta\vartheta_i^* = 0 \quad (5)
\end{aligned}$$

We show in Appendix B that all fixed points with indices in q are unstable. Therefore, all attractors are well-separated fixed points with $i \in p \forall i$.

Only fixed points with $\sin\Delta\vartheta_i^* = 0 \forall i$ and $\sum_{j=1}^N S_{ij} \cos\Delta\vartheta_j^* - M/2 \cos\Delta\vartheta_i^* \neq 0$ remain as candidates for attractors.

The stability of fixed points can generally be examined by linearizing the dynamics around the fixed point by evaluating the eigenvalues of the Jacobian $J_{ik} = \partial\Delta\dot{\vartheta}_i/\partial\Delta\vartheta_k$ at the fixed point $\Delta\vec{\vartheta}^*$:

$$\begin{aligned}
J_{ik} = & -\frac{\epsilon}{N} \cos\Delta\vartheta_i \delta_{ik} \left(\sum_{j=1}^N S_{ij} \cos\Delta\vartheta_j - \frac{M}{2} \cos\Delta\vartheta_i \right) \\
& - \frac{\epsilon}{N} \sin\Delta\vartheta_i \left(-S_{ik} \sin\Delta\vartheta_l + \frac{M}{2} \delta_{ik} \sin\Delta\vartheta_i \right)
\end{aligned}$$

As $i \in p \forall i$ implies $\sin\Delta\vartheta_i^* = 0 \forall i$, the second term vanishes:

$$J_{ik}(\Delta\vec{\vartheta}^*) = -\delta_{ik} \frac{\epsilon}{N} \cos\Delta\vartheta_i^* \left(\sum_{j=1}^N S_{ij} \cos\Delta\vartheta_j^* - \frac{M}{2} \cos\Delta\vartheta_i^* \right)$$

\mathbf{J} is a diagonal matrix, therefore eigenvectors \hat{e}_i are the standard base with the following eigenvalues:

$$\lambda_i = -\frac{\epsilon}{N} \cos\Delta\vartheta_i^* \left(\sum_{j=1}^N S_{ij} \cos\Delta\vartheta_j^* - \frac{M}{2} \cos\Delta\vartheta_i^* \right)$$

We can simplify the analysis further by defining "pattern coordinates" $\vec{\alpha}$ with $\alpha_i = \cos\Delta\vartheta_i$ as generalization

of Eq. 3 and inserting the definition of the coupling matrix \mathbf{S} :

$$\begin{aligned}
\lambda_i = & -\frac{\epsilon}{N} \left(\sum_{m=1}^M \alpha_i^m \alpha_i^* \sum_{j=1}^N \alpha_j^m \alpha_j^* - \frac{M}{2} \alpha_i^{*2} \right) \\
= & -\frac{\epsilon}{N} \left(\sum_{m=1}^M \alpha_i^m \alpha_i^* \langle \vec{\alpha}^m, \vec{\alpha}^* \rangle - \frac{M}{2} \right)
\end{aligned}$$

The signs of the eigenvalues determine the stability: Positive eigenvalues denote growing perturbations along the corresponding eigendirection, while negative eigenvalues indicate decay. Therefore, all fixed points with $\lambda_i < 0 \forall i$ are isolated attractors:

$$\sum_{m=1}^M \alpha_i^m \alpha_i^* \langle \vec{\alpha}^m, \vec{\alpha}^* \rangle > \frac{M}{2} \quad \wedge \quad \alpha_i^* \in \{\pm 1\} \quad (6)$$

Memorized patterns map to isolated attractors, if inter-pattern scalar products are sufficiently small. If patterns $\vec{\alpha}^m$ are orthogonal, inter-pattern scalar products vanish completely:

$$\begin{aligned}
\lambda_i(\vec{\alpha}^{m'}) = & -\frac{\epsilon}{N} \left(\sum_{m=1}^M \alpha_i^m \alpha_i^{m'} \langle \vec{\alpha}^m, \vec{\alpha}^{m'} \rangle - \frac{M}{2} \right) \\
= & -\frac{\epsilon}{N} \left(\sum_{m=1}^M \alpha_i^m \alpha_i^{m'} \delta_{mm'} N - \frac{M}{2} \right) \\
= & -\epsilon \left(1 - \frac{M}{2N} \right) < 0 \quad \forall i \\
\Leftrightarrow & M < 2N
\end{aligned}$$

Not more than N orthogonal patterns can exist ($\text{span}(\vec{\alpha}^m) \leq N$, but $\text{span}(\vec{\alpha}^m) = M$ for linear independent patterns.), so $M < 2N$ is always fulfilled and orthogonal patterns are guaranteed to be stable.

For general $\vec{\alpha}^m$, we get

$$\begin{aligned}
& \lambda_i(\vec{\alpha}^{m'}) \stackrel{!}{<} 0 \\
-\epsilon - \frac{\epsilon}{N} \left(\sum_{m \neq m'}^M \alpha_i^m \alpha_i^{m'} \langle \vec{\alpha}^m, \vec{\alpha}^{m'} \rangle - \frac{M}{2} \right) & < 0 \\
& - \sum_{m \neq m'}^M \alpha_i^m \alpha_i^{m'} \langle \vec{\alpha}^m, \vec{\alpha}^{m'} \rangle < N - \frac{M}{2}.
\end{aligned}$$

As we want a criterion to ensure that all memorized patterns are attractors, we must exclude that any eigendirection of any pattern becomes unstable:

$$\begin{aligned}
\max_{i, m'} \left(- \sum_{m \neq m'}^M \alpha_i^m \alpha_i^{m'} \langle \vec{\alpha}^m, \vec{\alpha}^{m'} \rangle \right) & < N - \frac{M}{2} \\
\Sigma_{max} \stackrel{!}{=} \max_{m'} \left(\sum_{m \neq m'}^M |\langle \vec{\alpha}^m, \vec{\alpha}^{m'} \rangle| \right) & < N - \frac{M}{2}
\end{aligned}$$

Additionally, if the $\vec{\alpha}^m$ are attractors, their *inverses will be attractors as well* because their eigenvalues are identical:

$$\begin{aligned}\lambda_i(-\vec{\alpha}^{m'}) &= -\frac{\epsilon}{N} \left[\sum_{m=1}^M \alpha_i^m (-\alpha_i^{m'}) \langle \vec{\alpha}^m, (-\vec{\alpha}^{m'}) \rangle - \frac{M}{2} \right] \\ &= -\frac{\epsilon}{N} \left(\sum_{m=1}^M \alpha_i^m \alpha_i^{m'} \langle \vec{\alpha}^m, \vec{\alpha}^{m'} \rangle - \frac{M}{2} \right) \\ &= \lambda_i(\vec{\alpha}^{m'})\end{aligned}$$

Furthermore, there are further spurious attractors that do not represent one of the $\vec{\alpha}^m$, but they are difficult to describe. If the initial pattern does not start in the basin of attraction of an $\vec{\alpha}^m$, the output of the system will be one of these attractors. Therefore, stability is not sufficient for recognition success and we have to derive a criterion from the basins of attraction.

C. Intuitive explanation of the recognition mechanism

The results of the fixed point analysis allow a more intuitive view of Eq. (4) by partially expressing the system state in pattern coordinates $\vec{\alpha}$ with $\alpha_i = \cos \Delta\vartheta_i$:

$$\begin{aligned}\Delta\dot{\vartheta}_i &= -\frac{\epsilon}{N} \sin \Delta\vartheta_i \left(\sum_{j=1}^N S_{ij} \cos \Delta\vartheta_j - \frac{M}{2} \cos \Delta\vartheta_i \right) \\ &= -\frac{\epsilon}{N} \sin \Delta\vartheta_i \left(\sum_{j=1}^N \sum_{m=1}^M \alpha_i^m \alpha_j^m \alpha_j - \frac{M}{2} \alpha_i \right) \\ &= -\sin \Delta\vartheta_i \cdot \frac{\epsilon}{N} \left(\sum_{m=1}^M \alpha_i^m \langle \vec{\alpha}^m, \vec{\alpha} \rangle - \frac{M}{2} \alpha_i \right)\end{aligned}$$

Let us neglect $-M\alpha_i/2$ at first as it vanishes in the limit $N \rightarrow \infty$ and assume the system state $\vec{\alpha}$ is sufficiently close to a memorized pattern $\vec{\alpha}^{m'}$: Then $\langle \vec{\alpha}^{m'}, \vec{\alpha} \rangle$ is larger than the rest of the sum and $\text{sgn}(\sum_{m=1}^M \alpha_i^m \langle \vec{\alpha}^m, \vec{\alpha} \rangle) = \alpha_i^{m'}$, so the fixed points and their stability are the same as in $d/dt \Delta\vartheta_i = -\alpha_i^{m'} \sin \Delta\vartheta_i$. If $\alpha_i^{m'} = +1$, $\Delta\vartheta_i^* = 0$ is stable and $\Delta\vartheta_i^* = \pi$ is unstable and vice-versa for $\alpha_i^{m'} = -1$, so $\lim_{t \rightarrow \infty} \alpha_i = \cos \Delta\vartheta_i^* = \alpha_i^{m'}$.

From another point of view, the system "defines" "relative closeness" to memorized patterns by comparing their projections onto the system state $\vec{\alpha}$. This fails, however, if the scalar products are of comparable size: Then the distribution of the α_i^m matters for each pixel, which leads to spurious attractors unequal to all $\vec{\alpha}^m$. Finally, the $-M\alpha_i/2$ -term does not really contribute to the recognition mechanism. While it increases eigenvalues of all stable fixed points slightly, therefore reducing stability, it does not influence the basins of attraction much, as we will illustrate in the next section.

IV. BASINS OF ATTRACTION AND GUARANTEED RECOGNITION

We have a firm understanding of the system now and can guarantee that the chosen patterns $\vec{\alpha}^m$ are attractive. However, we cannot guarantee recognition success yet: The system state might relax to the additional unwanted attractors described by Eq. (6) or even worse, the basins of attraction of the $\vec{\alpha}^m$ might be malformed, leading to a $\vec{\alpha}^m$ whose projection on the defective pattern is not the largest.

A. Lower bound on the basins of attraction

Matching success is guaranteed if the defective starting pattern is in the basin of attraction of the correct memorized pattern $\vec{\alpha}^{m'}$. A lower bound on the basin of attraction can be derived by proofing the following lemmata:

1. Surfaces of constant projection on the correct memorized pattern $\vec{\alpha}^{m'}$ confine the system state to larger projections if the initial projection is sufficiently large.
2. $\vec{\alpha}^{m'}$ is the only attractor inside this confined space.

As the system state cannot leave the confined space, it has to settle on $\vec{\alpha}^{m'}$ as the only attractor. Therefore, the confined space is part of $\vec{\alpha}^{m'}$'s basin of attraction.

1. Transformation to $\vec{\alpha}$ -space

For our following discussion, we will transfer the $\Delta\vec{\vartheta}_i$ -dynamics (Eq. (4)) completely into the "pattern coordinates" $\vec{\alpha}$ with $\alpha_i = \cos \Delta\vartheta_i$, which are a generalization of the mapping of the memorized patterns $\vec{\alpha}^m$.

$$\begin{aligned}\dot{\alpha}_i &= (\cos \Delta\vartheta_i) \\ &= \frac{\partial \cos \Delta\vartheta_i}{\partial \Delta\vartheta_i} \frac{\partial \Delta\vartheta_i}{\partial t} \\ &= -\sin \Delta\vartheta_i \left[-\frac{\epsilon}{N} \sin \Delta\vartheta_i \left(\sum_{j=1}^N S_{ij} \cos \Delta\vartheta_j - \frac{M}{2} \cos \Delta\vartheta_i \right) \right] \\ &= \frac{\epsilon}{N} \sin^2 \Delta\vartheta_i \left(\sum_{j=1}^N \sum_{m=1}^M \alpha_i^m \alpha_j^m \cos \Delta\vartheta_j - \frac{M}{2} \cos \Delta\vartheta_i \right)\end{aligned}$$

$$\begin{aligned}
&= \frac{\epsilon}{N} (1 - \cos^2 \Delta\vartheta_i) \left(\sum_{j=1}^N \sum_{m=1}^M \alpha_i^m \alpha_j^m \cos \Delta\vartheta_j \right. \\
&\quad \left. - \frac{M}{2} \cos \Delta\vartheta_i \right) \\
&= \frac{\epsilon}{N} (1 - \alpha_i^2) \left(\sum_{m=1}^M \alpha_i^m \sum_{j=1}^N \alpha_j^m \alpha_j - \frac{M}{2} \alpha_i \right) \\
\alpha_i &= \frac{\epsilon}{N} (1 - \alpha_i^2) \left(\sum_{m=1}^M \alpha_i^m \langle \vec{\alpha}^m, \vec{\alpha} \rangle - \frac{M}{2} \alpha_i \right) \quad (7)
\end{aligned}$$

Note that although the mapping between $\Delta\vartheta_i$ and α_i is *not* injective, the transformation is still valid: Eq. (4) is mirror-symmetric to $0 + \pi n$ with $n \in \mathbb{N}$, so space can be divided into regions separated by $\Delta\vartheta_i = [0, \pi] + 2\pi n$ or $\Delta\vartheta_i = [\pi, 2\pi] + 2\pi n$ in every i and flow lines in each region are mapped onto the same $\vec{\alpha}$ -coordinates. As the flow across the boundaries of these hypercubes is zero, it is not necessary to consider the periodicity of the flow. From another point of view, the ambiguity of attractors in $\Delta\vec{\vartheta}$ is removed in the $\vec{\alpha}$ -coordinates. As the dynamics of $\vec{\alpha}$ do not depend on the sign or periodicity of $\Delta\vec{\vartheta}$, it is a more natural coordinate for the autoassociative memory.

2. Confinement by hypersurfaces of constant projection

Let's consider a hypersurface of constant projection on the correct output pattern $\vec{\alpha}^{m'}$: In the pattern coordinates the equation $\langle \vec{\alpha}, \vec{\alpha}^{m'} \rangle = C$ describes a hyperplane that divides the N -dimensional hypercube of all possible patterns into patterns with a projection larger or smaller than C . If projections on $\vec{\alpha}^{m'}$ grow for all points on the surface, the system state can only move tangential to the hyperplane or towards larger projections. (Movement tangential to the hyperplane is in fact impossible with a slightly stricter condition, as shown further below.)

$$\begin{aligned}
&\frac{d}{dt} \frac{1}{|\vec{\alpha}^{m'}|} \langle \vec{\alpha}, \vec{\alpha}^{m'} \rangle \geq 0 \\
&\frac{d}{dt} \langle \vec{\alpha}, \vec{\alpha}^{m'} \rangle = \langle \dot{\vec{\alpha}}, \vec{\alpha}^{m'} \rangle \geq 0 \\
\sum_{i=1}^N (1 - \alpha_i^2) \alpha_i^{m'} \left(\sum_{m=1}^M \alpha_i^m \langle \vec{\alpha}^m, \vec{\alpha} \rangle - \frac{M}{2} \alpha_i \right) &\geq 0 \quad (8)
\end{aligned}$$

If Eq. (8) is fulfilled for all $\vec{\alpha}$ on a hypersurface $\langle \vec{\alpha}, \vec{\alpha}^{m'} \rangle = C$, it confines the system state. However, to exclude additional attractors besides $\vec{\alpha}^{m'}$ in the confined space is difficult with Eq. 8 and a good criterion for guaranteed recognition should neither depend on the hyperplanes nor on the specific pixels of $\vec{\alpha}$ or the memorized patterns $\vec{\alpha}^m$. Therefore, we employ a series of *worst-case approximations and upper bounds*:

Eq. 8 is fulfilled if all single summands are greater than zero. Note that this approximation also ex-

cludes movement tangential to the hypersurfaces: Without the possibility for summands to cancel each other, $d/dt \langle \vec{\alpha}, \vec{\alpha}^{m'} \rangle = 0$ is only fulfilled if $\dot{\vec{\alpha}} = 0$, so all remaining solutions are fixed points. Then the following inequalities must hold $\forall i$ and $\forall \vec{\alpha}$ on the surface:

$$\begin{aligned}
\underbrace{(1 - \alpha_i^2)}_{\geq 0} \alpha_i^{m'} \left(\sum_{m=1}^M \alpha_i^m \langle \vec{\alpha}^m, \vec{\alpha} \rangle - \frac{M}{2} \alpha_i \right) &\geq 0 \\
\alpha_i^{m'} \sum_{m=1}^M \alpha_i^m \langle \vec{\alpha}, \vec{\alpha}^m \rangle - \frac{M}{2} \alpha_i^{m'} \alpha_i &\geq 0
\end{aligned}$$

$$\langle \vec{\alpha}, \vec{\alpha}^{m'} \rangle \geq - \sum_{\substack{m=1 \\ m \neq m'}}^M \alpha_i^m \alpha_i^{m'} \langle \vec{\alpha}, \vec{\alpha}^m \rangle + \frac{M}{2} \alpha_i^{m'} \alpha_i$$

As the left hand side is constant on a hypersurface, the criterion needs to be evaluated for a maximized right hand side only and the criterion for the surface can be reduced to one single inequality:

$$\langle \vec{\alpha}, \vec{\alpha}^{m'} \rangle \geq \max_{i, \vec{\alpha}} \left(- \sum_{\substack{m=1 \\ m \neq m'}}^M \alpha_i^m \alpha_i^{m'} \langle \vec{\alpha}, \vec{\alpha}^m \rangle + \frac{M}{2} \alpha_i^{m'} \alpha_i \right)$$

The sum is maximal in i for $\alpha_i^m = -\alpha_i^{m'} \operatorname{sgn}(\langle \vec{\alpha}, \vec{\alpha}^m \rangle)$ $\forall m \neq m'$, as all scalar products add up. (If such an i always exists is not relevant here, as we look for a worst case approximation independent of the $\vec{\alpha}^m$.) The second term is generally much smaller, but $M/2$ at most:

$$\begin{aligned}
&\max_{i, \vec{\alpha}} \left(- \sum_{\substack{m=1 \\ m \neq m'}}^M \alpha_i^m \alpha_i^{m'} \langle \vec{\alpha}, \vec{\alpha}^m \rangle + \frac{M}{2} \alpha_i^{m'} \alpha_i \right) \\
&\leq \max_{\vec{\alpha}} \left(\sum_{\substack{m=1 \\ m \neq m'}}^M |\langle \vec{\alpha}, \vec{\alpha}^m \rangle| + \frac{M}{2} \right)
\end{aligned}$$

As the maximum of one single $|\langle \vec{\alpha}, \vec{\alpha}^m \rangle|$ is much easier to calculate, we approximate an upper bound:

$$\begin{aligned}
&\max_{\vec{\alpha}} \left(\sum_{\substack{m=1 \\ m \neq m'}}^M |\langle \vec{\alpha}, \vec{\alpha}^m \rangle| + \frac{M}{2} \right) \\
&\leq \sum_{\substack{m=1 \\ m \neq m'}}^M \max_{\vec{\alpha}} (|\langle \vec{\alpha}, \vec{\alpha}^m \rangle|) + \frac{M}{2}
\end{aligned}$$

In total, our criterion on the hypersurface has reduced to

$$C = \langle \vec{\alpha}, \vec{\alpha}^{m'} \rangle \leq \sum_{\substack{m=1 \\ m \neq m'}}^M \max_{\vec{\alpha}} (|\langle \vec{\alpha}, \vec{\alpha}^m \rangle|) + \frac{M}{2}. \quad (9)$$

While any hyperplane that fulfills Eq. (9) confines the system state to larger projections, it is still not trivial to evaluate due to the direct dependence on $\vec{\alpha}$.

3. Removing direct dependence on $\vec{\alpha}$

$\max_{\vec{\alpha}} (|\langle \vec{\alpha}, \vec{\alpha}^{m'} \rangle|)$ can be approximated as a function of $\langle \vec{\alpha}, \vec{\alpha}^{m'} \rangle = C$ and inter-pattern scalar products.

First, $\langle \vec{\alpha}, \vec{\alpha}^{m'} \rangle$ is expressed with the difference vector $\Delta \vec{\alpha} = \vec{\alpha} - \vec{\alpha}^{m'}$ between $\vec{\alpha}$ and the closest memorized pattern $\vec{\alpha}^{m'}$:

$$\begin{aligned} \langle \vec{\alpha}, \vec{\alpha}^{m'} \rangle &= \langle \vec{\alpha} - \vec{\alpha}^{m'}, \vec{\alpha}^{m'} \rangle + \langle \vec{\alpha}^{m'}, \vec{\alpha}^{m'} \rangle \\ &= \langle \Delta \vec{\alpha}, \vec{\alpha}^{m'} \rangle + N \\ &= \sum_{i=1}^N \Delta \alpha_i \alpha_i^{m'} + N \end{aligned}$$

With $\text{sgn}(\Delta \alpha_i) = \text{sgn}(\alpha_i^{m'} (\underbrace{\alpha_i \alpha_i^{m'}}_{\leq 1} - 1)) = -\alpha_i^{m'}$ we get:

$$\langle \vec{\alpha}, \vec{\alpha}^{m'} \rangle = N - \sum_{i=1}^N |\Delta \alpha_i| \quad (10)$$

$$\begin{aligned} \Rightarrow \max_{\vec{\alpha}} (|\langle \vec{\alpha}, \vec{\alpha}^{m'} \rangle|) &= \max_{\Delta \vec{\alpha}} (|\langle \Delta \vec{\alpha}, \vec{\alpha}^{m'} \rangle + \langle \vec{\alpha}^{m'}, \vec{\alpha}^{m'} \rangle|) \\ &< \max_{\Delta \vec{\alpha}} \left(\sum_i \Delta \alpha_i \alpha_i^{m'} \right) + |\langle \vec{\alpha}^{m'}, \vec{\alpha}^{m'} \rangle| \\ &= \sum_i |\Delta \alpha_i| + |\langle \vec{\alpha}^{m'}, \vec{\alpha}^{m'} \rangle| \\ &= N - \langle \vec{\alpha}, \vec{\alpha}^{m'} \rangle + |\langle \vec{\alpha}^{m'}, \vec{\alpha}^{m'} \rangle| \end{aligned}$$

4. Volumes of growing projection

Finally, we can remove all direct dependence on $\vec{\alpha}$ from Eq. (9):

$$\langle \vec{\alpha}, \vec{\alpha}^{m'} \rangle \geq \sum_{\substack{m=1 \\ m \neq m'}}^M \max_{\vec{\alpha}} (|\langle \vec{\alpha}, \vec{\alpha}^m \rangle|) + \frac{M}{2}$$

$$\langle \vec{\alpha}, \vec{\alpha}^{m'} \rangle \geq \sum_{\substack{m=1 \\ m \neq m'}}^M \left(N - \langle \vec{\alpha}, \vec{\alpha}^m \rangle + |\langle \vec{\alpha}^m, \vec{\alpha}^m \rangle| \right) + \frac{M}{2}$$

$$M \cdot \langle \vec{\alpha}, \vec{\alpha}^{m'} \rangle \geq (M-1) \cdot N + \sum_{\substack{m=1 \\ m \neq m'}}^M |\langle \vec{\alpha}^m, \vec{\alpha}^m \rangle| + \frac{M}{2}$$

$$\langle \vec{\alpha}, \vec{\alpha}^{m'} \rangle \geq \frac{M-1}{M} \cdot N + \frac{1}{M} \sum_{\substack{m=1 \\ m \neq m'}}^M |\langle \vec{\alpha}^m, \vec{\alpha}^m \rangle| + \frac{1}{2} \quad (11)$$

This final criterion for a confining hyperplane does not depend on a point on the surface.

Additionally, every surface $\langle \vec{\alpha}, \vec{\alpha}^{m'} \rangle = C_{min}$ that fulfills Eq. (11) defines a *volume of growing projection* for

larger C : As the right hand side of Eq. (11) is constant, all hyperplanes with $C > C_{min}$ fulfill the criterion as well.

If several attractors existed in the confined space, however, no conclusion could be made on the basins of attraction, as a confined system state could move to any of them. Therefore, we exclude that any attractor besides $\vec{\alpha}^{m'}$ exists in a volume of growing projection:

5. $\vec{\alpha}^{m'}$ being the only attractor enclosed

Assume an attractor $\vec{\alpha}^a$ exists inside the region defined by Eq. (11). Now consider a small perturbation around $\vec{\alpha}^a$ that increases $\langle \vec{\alpha}, \vec{\alpha}^{m'} \rangle$, for example $\epsilon \alpha_i^{m'} \cdot \hat{e}_i$ if $\alpha_i^a \neq \alpha_i^{m'}$. As $d/dt \langle \vec{\alpha}, \vec{\alpha}^{m'} \rangle \geq 0$ in the confined space, the system cannot relax back to $\vec{\alpha}^a$. No nonisolated attractor exists (see Sec. III), so $\vec{\alpha}^a$ has at least one unstable eigendirection which contradicts the assumption that $\vec{\alpha}^a$ is an attractor.

The only exception is the attractor $\vec{\alpha}^{m'}$ itself: As it has the largest projection on itself, all perturbations must lower $\langle \vec{\alpha}, \vec{\alpha}^{m'} \rangle$.

Summing up: Every system state $\vec{\alpha}$ that obeys Eq. (11) must be in the basin of attraction of $\vec{\alpha}^{m'}$, as projection on $\vec{\alpha}^{m'}$ increases monotonically along the trajectory and $\vec{\alpha}^{m'}$ is the only attractor for larger projections.

B. Guaranteed recognition

1. Recognition criteria

As any defective initialized pattern is binary, it can be characterized by the number of defective pixels n^f in which defective input pattern and correct memorized pattern are different. Eq. (11) can be solved for n^f with Eq. (10), as n^f is a special case of $\sum_i |\Delta \alpha_i|/2$:

$$\begin{aligned} N - 2n^f &> \frac{M-1}{M} \cdot N + \frac{1}{M} \sum_{\substack{m=1 \\ m \neq m'}}^M |\langle \vec{\alpha}^m, \vec{\alpha}^m \rangle| + \frac{1}{2} \\ n^f &< \frac{1}{2M} \left(N - \sum_{\substack{m=1 \\ m \neq m'}}^M |\langle \vec{\alpha}^m, \vec{\alpha}^m \rangle| \right) - \frac{1}{4} \quad (12) \end{aligned}$$

(The equality in Eq. (11) must be dropped here, as perturbations and higher order terms neglected in Eq. (4) might push a defective pattern on the outermost hyperplane out of the confined space.)

For *pairwise orthogonal patterns*, $\langle \vec{\alpha}^m, \vec{\alpha}^m \rangle = 0 \forall m \neq m'$ and Eq. (12) becomes:

$$\boxed{n^f < \frac{N}{2M} - \frac{1}{4}} \quad (13)$$

We now treat *general patterns* with $\langle \vec{\alpha}^{m'}, \vec{\alpha}^m \rangle \neq 0$. A criterion that does not depend on the correct memorized pattern $\vec{\alpha}^{m'}$ is obtained with the definition $\Sigma_{max} = \max_{\vec{\alpha}^{\bar{m}}} (\sum_{m=1, m \neq \bar{m}}^M |\langle \vec{\alpha}^{\bar{m}}, \vec{\alpha}^m \rangle|) > \sum_{m=1, m \neq m'}^M |\langle \vec{\alpha}^{m'}, \vec{\alpha}^m \rangle|$ from Sec. III. Then the worst case of Eq. (12) is

$$n^f < \frac{N - \Sigma_{max}}{2M} - \frac{1}{4}. \quad (14)$$

Eq. (14) guarantees successful recognition for arbitrary patterns.

2. Consistency Check

The basin of attraction has to vanish when the fixed point loses stability. Therefore, we can regain stability criteria for the $\vec{\alpha}^m$ by minimizing the necessary extension of the basin of attraction in Eq. (13) and Eq. (14), which corresponds to $\lim_{n^f \rightarrow 0}$:

$$M < \frac{N}{2n^f + \frac{1}{2}} \quad \Big| \lim_{n^f \rightarrow 0}$$

$$\Rightarrow M < 2N$$

This coincides with our calculation that pairwise orthogonal patterns are always stable: At most, N orthogonal patterns can exist, as they are linear independent and $\dim(\text{span}(\{\vec{\alpha}^m\})) \leq N$, so $M < 2N$ is always fulfilled.

$$\frac{M}{N} < \frac{1 - \frac{\Sigma_{max}}{N}}{2n^f + \frac{1}{2}} \quad \Big| \lim_{n^f \rightarrow 0}$$

$$\frac{M}{2N} < 1 - \frac{\Sigma_{max}}{N}$$

$$\Sigma_{max} < N - \frac{M}{2}$$

This again reproduces our result for the stability of nonorthogonal patterns.

V. NUMERICAL SIMULATIONS

In this section we validate our criterion for successful pattern recognition with simulations of the full phase dynamics Eq. (1).

A. Numerical methods and parameters

The equations have been implemented in C and integration was performed with the classical Runge-Kutta method. A timestep $dt = 1 \cdot 10^{-4}$ and a coupling strength $\epsilon = 0.4$ were used. The frequencies were distributed according to $f_i = 1200 + 1800 \cdot G_i / G_N$, where G_i is the i -th

n^f	6-11	12	13	14	15	16
failed recognitions ♥	0	0	0	1	5	13
failed recognitions ♠	0	2	2	3	3	15
failed recognitions π	0	1	2	6	6	22
failure rate	0%	0.3%	0.4%	1.1%	1.6%	5.6%

FIG. 5. Failed Recognitions with nonorthogonal patterns as shown in Fig. 2. 300 recognitions were performed for each pattern and each number of erroneous pixels n^f . Erroneous pixels were distributed randomly for each simulation.

element of a Golomb ruler [26] (see also Appendix A). The near optimal Golomb rulers used were both taken from [27]: $\{0, 17, 20, 86, 119, 140, 166, 227, 240, 255, 353, 430, 520, 559, 564, 565, 602, 675, 724, 781, 817, 833, 905, 929, 961, 970, 980, 1131, 1162, 1189, 1212, 1319, 1403, 1433, 1437, 1451, 1462, 1497, 1504, 1589, 1601, 1680, 1763, 1785, 1825, 1880, 1888, 1956, 1958\}$ for $N = 49$ and $\{0, 34, 44, 91, 95, 147, 207, 278, 332, 364, 375, 405, 458, 520, 682, 698, 701, 710, 853, 868, 901, 946, 973, 1022, 1080, 1150, 1155, 1172, 1240, 1254, 1290, 1429, 1540, 1546, 1605, 1642, 1682, 1684, 1705, 1751, 1771, 1806, 1835, 1943, 1967, 2041, 2151, 2164, 2182, 2189, 2190, 2270\}$ for $N = 52$.

For simulations in Fig. 3 and Fig. 4, defective patterns were chosen manually and memorized patterns are taken from Fig. 2. All pseudorandom numbers (necessary for random distribution of erroneous pixels and construction of random orthogonal patterns) were created using C's standard random number generator `rand()` from `stdlib`, which was seeded with the time in microseconds times the process ID.

B. Testing criteria for guaranteed recognition

In order to test criteria Eq. (13) and (14), simulations were performed for both the nonorthogonal patterns shown in Fig. 2 with $N=49$ pixels as well as for 3 random orthogonal patterns with $N=52$ pixels. Simulations started after the initialization step with a defective pattern similar to one of the memorized patterns but different in exactly n^f randomly distributed erroneous pixels. In order to save simulation time, simulations were aborted if the system state reached one of the memorized patterns, as they are proven to be attractors. In all other cases, simulations were continued until $|\alpha_i| \geq 0.9 \forall i$ for a period $t_{wait} = 500$. Recognition success was tested by projecting the $\vec{\alpha}$ -coordinates of the final system state on the memorized patterns: If $\langle \vec{\alpha}, \vec{\alpha}^{m'} \rangle / N > 0.99$, recognitions were counted as successful.

For the nonorthogonal patterns with $M = 3$, $N = 49$ and $\Sigma_{max} = 10$, the recognition criterion Eq. (14) predicts recognition success for $n^f < (N - \Sigma_{max}) / (2M) - 0.25 = 6.25$. 300 simulations were performed for $n^f \in \{6, 16\}$ for each pattern and results are summed up in Fig. 5. All recognitions were successful for $n^f \leq 11$ and

n^f	8-12	13	14	15	16	17
failed recognitions	0	1	1	4	13	29
failure rate	0%	0.1%	0.1%	0.4%	1.3%	2.9%

FIG. 6. Failed Recognitions with random orthogonal patterns with $N = 52$ pixels. 1000 recognitions were performed for each number of erroneous pixels n^f . Random distribution of erroneous pixels and the construction of random orthogonal patterns was repeated for each simulation.

the rate of failed recognitions grows slowly for larger n^f . Obviously, our criterion seems to be too strict.

Similarly, 1000 simulations were performed with orthogonal random patterns with $N = 52$ and $M = 3$ for each $n^f \in \{8..17\}$. Here, $n^f < N/(2M) - 0.25 = 8.42$ is predicted by Eq. (13). Random orthogonal patterns were constructed by using the elementwise product \circ : As orthogonal patterns with $\alpha_i \in \pm 1$ differ in exactly $N/2$ pixels, a pattern $\vec{\alpha}^2$ orthogonal to any pattern $\vec{\alpha}^1$ can be easily found by creating a "difference vector" $\vec{d}^{1,2}$, where $N/2 +1$ - and -1 -entries are randomly distributed. Then $\vec{\alpha}^2 = \vec{\alpha}^1 \circ \vec{d}^{1,2}$.

For 3 orthogonal patterns, $\vec{\alpha}^1$, $\vec{d}^{1,2}$ and $\vec{d}^{1,3}$ were first chosen randomly. Then $|\langle \vec{\alpha}^2, \vec{\alpha}^3 \rangle| = |\langle \vec{d}^{1,2}, \vec{d}^{1,3} \rangle|$ was minimized by switching 2 randomly selected pixels in a randomly selected difference vector, if the absolute value of the scalar product diminished.

Results are summed up in Fig. 6. Similar to the simulations with nonorthogonal patterns, failed recognitions are not found close to the maximal n^f predicted by the criterion for guaranteed recognition.

C. Failed recognitions are rare events

One might expect that the criterion for guaranteed recognition is not optimal for both the orthogonal random patterns and our choice of nonorthogonal patterns, so that 7 respectively 9 erroneous pixels or even more can always be correctly recognized as well. However, failed recognitions are just rare for $n^f = 7 / n^f = 9$ instead. We now construct problematic starting patterns with $n^f = 7$ for the nonorthogonal memorized patterns that fail in the recognition process:

According to Eq. (9), recognition will fail if the scalar products between the defective starting pattern and non-similar memorized patterns are extremized. Considering the scalar products $\langle \vec{\alpha}^\heartsuit, \vec{\alpha}^\pi \rangle = +5$, $\langle \vec{\alpha}^\heartsuit, \vec{\alpha}^\clubsuit \rangle = -5$, and $\langle \vec{\alpha}^\pi, \vec{\alpha}^\clubsuit \rangle = -1$, an erroneous heart-pattern is most likely to fail. Assume furthermore that the number of erroneous pixels n^f is fixed. Then the right hand side of Eq. (9) can be maximized by distributing the errors on positions where they increase the projection on the π - and decrease the projection on the \clubsuit -pattern. 10 such "worst-case" positions can be found for the \heartsuit -pattern and $\binom{10}{7} = 120$ possible combinations exist to distribute $n^f = 7$ erroneous pixels on the "worst-case" positions.

Simulations were performed for all of these "worst case patterns". Recognition failed for all simulations and the system state relaxed to an attractor with projections of 0.59, -0.51 and 0.51 on the \heartsuit -, \clubsuit - and π -pattern. Possible worst-case positions for erroneous pixels and the irregular output pattern are shown in Fig. 7. Indeed,

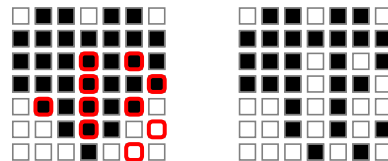


FIG. 7. On the left side, an unperturbed \heartsuit -pattern is shown. Erroneous pixels on red-circled positions extremize the sum of inter-pattern scalar products. All erroneous \heartsuit -patterns with 7 erroneous pixels on marked locations fail the recognition process. Simulations of all such patterns resulted in the spurious attractor shown on the right.

simulations with randomly distributed errors could not recognize this: As there are $\binom{49}{7} \approx 8,6 \cdot 10^7$ possibilities to distribute the erroneous pixel on the pattern and only $\binom{10}{7} = 120$ worst case distributions can be found, the chance to encounter a failing random starting pattern is almost negligible. Furthermore, all $\binom{10}{6} = 210$ worst-case-patterns for $n^f = 6$ were successfully recognized as the \heartsuit -pattern in simulations, which again validates Eq. (14) as criterion for guaranteed recognition. Similar calculations can be performed for the orthogonal case. This is a good example that extracting basins of attractions in high-dimensional systems with simulations can only give an approximation on the success rate but no guaranteed criterion. From another point of view, failed recognitions are rare, so a higher n^f is acceptable if a nonperfect recognition rate is sufficient.

VI. DISCUSSION

The above results revealed several features of the MONACO-architecture that are distinctive to this network. Firstly, though using the idea of time-dependent global coupling from refs. [15, 16] for an individual network, the use of two mirrored networks allows for the *internal* generation of the global coupling modulations. In contrast, the hardware implementation introduced in [16, 17] was fed by a computer-generated coupling modulation. Furthermore, readout is also considerably easier when compared to the latter two architectures. Instead of having to determine phase shifts or, more precisely, the mutual phase differences between the phase shifts of oscillators of different frequencies, only the phase differences between identical oscillators have to be determined. Beyond that, the dynamic always converges to an attractor that, independently of whether it is a memorized pattern or a spurious attractor, only contains '+1's and '-1's in pattern space $\vec{\alpha}$ (cf. Eq. (7)). This leads to a

further considerable simplification of readout. Another favorable consequence of the mirrored network is that the shift of frequency present in the real dynamics of the other mentioned Kuramoto-type networks [15, 16, 21, 24] does not interfere with the recognition process here since the change in frequency is identical in each oscillator pair.

The second essential modification is the use of a different coupling function. While traditional Kuramoto-type networks employ a coupling that depends only on the mutual phase differences of all oscillators ($\propto \sin(\vartheta_i - \vartheta_j)$), our coupling function is seemingly more complex (*cf.* Eq. (1) for the formulation in original phase variables and Eq. (4) for the formulation in phase differences). Yet, in pattern space $\vec{\alpha}$ it takes on a simple mathematical form, Eq. (7). The resulting dynamics bring about two substantial advantages: The ‘candidate patterns’ are *individual* attractors, while in the network with the classical coupling the individual patterns are connected by lines of attractive fixed points, rendering only short term recognition possible. Furthermore, the basins of attraction can be approximated analytically, allowing for the determination of the maximum possible number of defective pixels n^f as a function of the number of oscillators N and the number of memorized patterns M that leads to error-free guaranteed recognition.

Concerning quantitative measures for associative networks, often the capacity or loading rate of a network is used. It describes the maximum possible ratio of M and N , where memorized patterns still correspond to stable attractors. Usually it is computed for a set of random memorized patterns in the limit $N \rightarrow \infty$. This definition, however, includes deviations from the originally proposed mapping, so e.g. some bits may be erroneous at retrieval. Nishikawa et al. point out the importance of error-free retrieval for engineering applications [18] and suggest an error-free capacity as a more meaningful quantity. While we have not computed either of the two capacity measures yet, our recognition criterion (Eq. (14)) suggests yet another extension of the error-free capacity relating the number of allowed defective pixels n^f to M and N : If a network stores a large number of patterns, the basins of attraction will consequently be quite small and few erroneous pixels n^f can be corrected. In many applications, however, the number of patterns M is much smaller than N and the ability to correct larger errors is desired. While Eq. (14) might be evaluated for random patterns and $N \rightarrow \infty$, Eq. (14) already provides guaranteed predictions for applications with fixed $\vec{\alpha}^m$.

The last aspects to be discussed concern recognition time and oscillator accuracy. As mentioned in the introduction, a handicap of traditional networks, in particular the network based on identical Kuramoto oscillators, is the large number of physical connections scaling with $\mathcal{O}(N^2)$. This is overcome in the networks with time-dependent global coupling where only one connection per oscillator is needed, as used in [15–17] and also in the present case. However, the reduction in the number of spatial connections is not for free: The original com-

plexity in space is transferred to a complexity in time with the number of frequencies contained in the coupling modulation growing like $\mathcal{O}(N^2)$. Since in practice there will be only a certain frequency interval available, the recognition time scales with $\mathcal{O}(N^2)$ and the number of oscillators is limited by the accuracy of the frequencies [16]. However, it is likely that the same modifications on the original globally coupled Kuramoto network realized in [17] can also be introduced in the MONACO-architecture. In this improved network, physical connections still scale with $\mathcal{O}(N)$, but recognition time scales only with $\mathcal{O}(N^{\ln(3)/\ln(2)})$.

VII. SUMMARY & OUTLOOK

We presented a network of coupled nonlinear oscillators as a new architecture for an autoassociative memory device. Two subnetworks of oscillators with equal frequency distributions are each globally coupled. An additional temporal modulation of the coupling is constructed from signals of oscillators in the other subnetwork and the binary memorized patterns. The oscillator pairs of equal frequency synchronize to phase shifts of either 0 or π , which corresponds to the pixel values of a binary output pattern. Furthermore, the number of connections scales linearly with the number of pixels N and the only necessary input are defective pattern and memorized patterns. While orthogonal memorized patterns are always attractors, general memorized patterns are stable as well if their projections on each other are not too large. Although spurious attractors also exist, we derived a simple criterion for guaranteed recognition from worst case approximations on the basins of attraction for orthogonal as well as general patterns. Finally, our results were confirmed by simulations, which also indicate that failed recognitions might occur but are quite rare as long as the criterion for guaranteed recognition is only weakly missed. While other oscillatory neural networks exist which scale linearly with the number of pixels N or have isolated attractors, our MONACO-architecture is the first to combine both features as well as the first to provide solid criteria for guaranteed recognition.

Several questions remain open: The coupling strength ϵ needs to be increased as much as possible for fast recognition times. Additionally, the system’s robustness to frequency deviations or noise is unknown and might be addressed both theoretically or experimentally. In principle, a hardware realization is independent of the exact type of oscillator as long as their signal shape is close to harmonic. Thus, also fast state-of-the-art nanoo oscillators [28, 29] are conceivable. In this context, the influence of small delays should be discussed.

Finally, an even better time-connection tradeoff might be possible: Distributing frequency components on multiple coupling modulations similar to [17] might provide better scaling of recognition time combined with all the other benefits of our architecture.

ACKNOWLEDGMENTS

We want to thank Alexander Sparber and Stefan Litzel for fruitful discussions and careful reading. Furthermore, we thank the Nanosystems Initiative Munich (NIM) for financial support.

Appendix A: Averaging and frequency restrictions

In this Appendix, we apply the method of averaging [25] to the phase description Eq. 1. Therefore, we first expand the products in Eq. (1) with the trigonometric equalities $\sin x \cos y = [\sin(x-y) + \sin(x+y)]/2$ and $\sin x \sin y = [\cos(x-y) - \cos(x+y)]/2$ to obtain all frequency components:

$$\begin{aligned}
\dot{\vartheta}_i^{[1]} - \Omega_i &= \\
&= \frac{\epsilon}{N} \cos \vartheta_i^{[1]} \cdot \sum_{j=1}^N a^{[2]}(t) \sin \vartheta_j^{[1]} \\
&= \frac{\epsilon}{N} \sum_{j,k,l=1}^N S_{lk} \sin \vartheta_l^{[2]} \cos \vartheta_i^{[1]} \cdot \sin \vartheta_j^{[1]} \sin \vartheta_k^{[2]} \\
&= \frac{\epsilon}{4N} \sum_{j,k,l=1}^N S_{lk} \left[\sin(\vartheta_l^{[2]} - \vartheta_i^{[1]}) + \sin(\vartheta_l^{[2]} + \vartheta_i^{[1]}) \right] \\
&\quad \cdot \left[\cos(\vartheta_j^{[1]} - \vartheta_k^{[2]}) - \cos(\vartheta_j^{[1]} + \vartheta_k^{[2]}) \right] \\
&= \frac{\epsilon}{8N} \sum_{j,k,l=1}^N S_{lk} \left[\begin{aligned} &\sin(\vartheta_l^{[2]} - \vartheta_i^{[1]} - \vartheta_j^{[1]} + \vartheta_k^{[2]}) \\ &+ \sin(\vartheta_l^{[2]} - \vartheta_i^{[1]} + \vartheta_j^{[1]} - \vartheta_k^{[2]}) \\ &- \sin(\vartheta_l^{[2]} - \vartheta_i^{[1]} - \vartheta_j^{[1]} - \vartheta_k^{[2]}) \\ &- \sin(\vartheta_l^{[2]} - \vartheta_i^{[1]} + \vartheta_j^{[1]} + \vartheta_k^{[2]}) \\ &+ \sin(\vartheta_l^{[2]} + \vartheta_i^{[1]} - \vartheta_j^{[1]} + \vartheta_k^{[2]}) \\ &+ \sin(\vartheta_l^{[2]} + \vartheta_i^{[1]} + \vartheta_j^{[1]} - \vartheta_k^{[2]}) \\ &- \sin(\vartheta_l^{[2]} + \vartheta_i^{[1]} - \vartheta_j^{[1]} - \vartheta_k^{[2]}) \\ &- \sin(\vartheta_l^{[2]} + \vartheta_i^{[1]} + \vartheta_j^{[1]} + \vartheta_k^{[2]}) \end{aligned} \right]
\end{aligned}$$

As $\vartheta_i^{[1/2]} = \Omega_i t + \mathcal{O}(\epsilon)$, each of the sin-terms might oscillate with frequencies of $\mathcal{O}(\Omega_i)$ or $\mathcal{O}(\Delta\Omega_{ij})$. ($\Delta\Omega_{ij} = \Omega_i - \Omega_j$) As the characteristic timescales $\mathcal{O}(\Omega_i^{-1})$ and $\mathcal{O}(\Delta\Omega_{ij}^{-1})$ are much smaller than ϵ^{-1} , the time average of these oscillating terms vanishes on times $\mathcal{O}(\epsilon^{-1}) \gg \mathcal{O}(\Delta\Omega_{ij}^{-1})$. If frequencies in the argument cancel each other out, however, the argument is constant on timescales $\mathcal{O}(\epsilon^{-1})$ and all oscillating terms are negligible. Depending on the signs in the sin-argument, there can be different possibilities how constant terms can arise:

In the first term, for example, frequencies cancel if $\Omega_l + \Omega_k = \Omega_i + \Omega_j$. That is always true for $l = i \wedge k = j$ or $l = j \wedge k = i$, imposing an interaction between the i -th and j -th oscillators in both networks depending on S_{ij} . However, frequencies might also cancel if the frequency distribution is chosen poorly, which would wrongly connect oscillators with different numbers i, j, k, l only dependent on S_{lk} . Therefore, we require $\Omega_l + \Omega_k \neq \Omega_m + \Omega_n \forall$ pairwise different l, k, m, n .

Similarly, the lowest order is obtained in the third term for $\Omega_l = \Omega_i + \Omega_j + \Omega_k$. In order to avoid interaction between the i -th and j -th oscillators based on S_{lk} again, the frequency distribution must obey $\Omega_l \neq \Omega_m + \Omega_n + \Omega_k \forall l, k, m, n$ and the third term becomes negligible as well as the fourth, fifth and sixth term.

While the eighth term averages out without further conditions, we get identical contributions from the second and the seventh term. This can be seen by renaming indices l and k and using $S_{lk} = S_{kl}$:

$$\begin{aligned}
\dot{\vartheta}_i^{[1]} - \Omega_i &\approx \\
&\approx \frac{\epsilon}{8N} \sum_{j,k,l=1}^N S_{lk} \left[\begin{aligned} &(\delta_{il}\delta_{kj} + \delta_{ik}\delta_{lj} - \delta_{ik}\delta_{kl}\delta_{lj}) \sin(\vartheta_l^{[2]} - \vartheta_i^{[1]} - \vartheta_j^{[1]} + \vartheta_k^{[2]}) \\ &+ 2\delta_{il}\delta_{kj} \sin(\vartheta_l^{[2]} - \vartheta_i^{[1]} + \vartheta_j^{[1]} - \vartheta_k^{[2]}) \end{aligned} \right] \\
&= \frac{\epsilon}{8N} \sum_{j=1}^N \left[\begin{aligned} &-S_{ij} \sin((\vartheta_i^{[1]} - \vartheta_i^{[2]}) + (\vartheta_j^{[1]} - \vartheta_j^{[2]})) \\ &-S_{ji} \sin((\vartheta_i^{[1]} - \vartheta_i^{[2]}) + (\vartheta_j^{[1]} - \vartheta_j^{[2]})) \\ &+ 2S_{ij} \sin((\vartheta_i^{[1]} - \vartheta_i^{[2]}) - (\vartheta_j^{[1]} - \vartheta_j^{[2]})) \end{aligned} \right] \\
&\quad + \frac{\epsilon}{8N} S_{ii} \sin(2(\vartheta_i^{[1]} - \vartheta_i^{[2]}))
\end{aligned}$$

Final simplifications can be obtained by introducing the phase difference of oscillators with identical frequency $\Delta\vartheta_i = \vartheta_i^{[1]} - \vartheta_i^{[2]}$ and using $S_{ji} = S_{ij}$ as well as $S_{ii} = M$. For $\dot{\vartheta}_i^{[2]}$, the calculation is the same with inverted upper indices:

$$\begin{aligned}
\dot{\vartheta}_i^{[1]} &= \Omega_i + \frac{\epsilon M}{8N} \sin(2\Delta\vartheta_i) \\
&\quad - \frac{\epsilon}{4N} \sum_{j=1}^N S_{ij} [\sin(\Delta\vartheta_i + \Delta\vartheta_j) + \sin(\Delta\vartheta_i - \Delta\vartheta_j)] \\
\dot{\vartheta}_i^{[2]} &= \Omega_i - \frac{\epsilon M}{8N} \sin(2\Delta\vartheta_i) \\
&\quad + \frac{\epsilon}{4N} \sum_{j=1}^N S_{ij} [\sin(\Delta\vartheta_i + \Delta\vartheta_j) + \sin(\Delta\vartheta_i - \Delta\vartheta_j)]
\end{aligned}$$

Remark:

As shown in [16], both conditions on the frequency distribution can be simplified further: (l, k, m, n are still pairwise different.)

$$\begin{aligned}
\Omega_l + \Omega_k &\neq \Omega_m + \Omega_n \\
\Omega_l - \Omega_n &\neq \Omega_m - \Omega_k \\
\Delta\Omega_{ln} &\neq \Delta\Omega_{mk}
\end{aligned}$$

All difference frequencies have to be different to each other. This can be fulfilled by multiplying the minimal difference frequency $\Delta\Omega_{min}$ with a Golomb-ruler [26], a set of integers with nonequal differences. Similarly, the second condition can be simplified to $\Omega_l - \Omega_m = \Delta\Omega_{lm} \neq \Omega_n + \Omega_k \forall l, k, m, n$. This last inequality is always fulfilled if $\Omega_{min} > \Omega_{max}/3$.

Appendix B: Ljapunov function and unstable fixed point sets

In this Appendix, we derive a Ljapunov function for Eq. (4). We use it to show that all fixed points with at least one index i that fulfills Eq. 5 are unstable.

1. Ljapunov function

First, we express Eq. (4) as a gradient system with potential U , where $\Delta\vartheta_i = -\partial U/\partial\Delta\vartheta_i \forall i$:

$$U = -\frac{\epsilon}{2N} \sum_{l=1}^N \left(\sum_{k=1}^N S_{kl} \cos \Delta\vartheta_k \cos \Delta\vartheta_l - \frac{M}{2} \cos^2 \Delta\vartheta_l \right)$$

This is equivalent to the overdamped motion of a particle in an energy landscape, where $\dot{\vec{v}} \propto -\vec{\nabla}E$. Therefore, U decreases along trajectories and is a Ljapunov-function, which ensures that fixed points are the only attractors possible in Eq. (4).

2. unstable fixed points

In order to prove that all fixed points with some $i \in q$ are unstable, we express the system state in pattern coordinates $\vec{\alpha}$ with $\alpha_i = \cos \Delta\vartheta_i$ and insert the coupling

matrix $S_{ij} = \sum_{m=1}^M \alpha_i^m \alpha_j^m$ into our potential function U :

$$\begin{aligned} U &= -\frac{\epsilon}{2N} \sum_{l=1}^N \left(\sum_{k=1}^N S_{kl} \cos \Delta\vartheta_k \cos \Delta\vartheta_l - \frac{M}{2} \cos^2 \Delta\vartheta_l \right) \\ &= -\frac{\epsilon}{2N} \sum_{k,l=1}^N \left(\sum_{m=1}^M \alpha_k^m \alpha_l^m \alpha_k \alpha_l - \frac{M}{2} \delta_{kl} \alpha_l^2 \right) \\ &= -\frac{\epsilon}{2N} \left(\sum_{m=1}^M \langle \vec{\alpha}^m, \vec{\alpha} \rangle^2 - \frac{M}{2} \langle \vec{\alpha}, \vec{\alpha} \rangle \right) \end{aligned}$$

Now consider a small perturbation $\gamma \hat{e}_i$ from a fixed point $\vec{\alpha}^*$ where $i \in q$:

$$\begin{aligned} U(\vec{\alpha}^* + \gamma \hat{e}_i) &= \\ &= -\frac{\epsilon}{2N} \left[\sum_{m=1}^M \left(\langle \vec{\alpha}^m, \vec{\alpha}^* \rangle + \underbrace{\langle \vec{\alpha}^m, \gamma \hat{e}_i \rangle}_{=\gamma \alpha_i^m} \right)^2 - \frac{M}{2} \langle \vec{\alpha}^*, \vec{\alpha}^* \rangle \right. \\ &\quad \left. + 2 \langle \vec{\alpha}^*, \gamma \hat{e}_i \rangle + \langle \gamma \hat{e}_i, \gamma \hat{e}_i \rangle \right] \\ &= U(\vec{\alpha}^*) - \underbrace{\frac{\epsilon\gamma}{N} \left(\sum_{m=1}^M \alpha_i^m \langle \vec{\alpha}^m, \vec{\alpha}^* \rangle - \frac{M}{2} \alpha_i^* \right)}_{=0, \text{ as } i \in q. (\text{see Eq. (5)})} \\ &\quad - \frac{\epsilon}{2N} \left(\sum_{m=1}^M \gamma^2 \underbrace{(\alpha_i^m)^2}_{=+1} - \frac{M}{2} \gamma^2 \right) \\ &= U(\vec{\alpha}^*) - \frac{\epsilon M}{4N} \gamma^2 \end{aligned}$$

As U decreases close to $\vec{\alpha}^*$, there must be an unstable eigendirection and the fixed point must be unstable if at least one i with $\sum_{j=1}^N S_{ij} \cos \Delta\vartheta_j^* - \frac{M}{2} \cos \Delta\vartheta_i^* = 0$ exists. (i.e. $i \in q$)

Therefore, only the isolated fixed points with $\sin \Delta\vartheta_i^* = 0 \forall i$ and $S_{ik} \sin \Delta\vartheta_k^* - M/2 \delta_{ik} \sin \Delta\vartheta_i^* \neq 0 \forall i$ can be attractors.

-
- [1] Arkady Pikovsky, Michael Rosenblum, and Jürgen Kurths, *Synchronization: a universal concept in nonlinear sciences*, Vol. 12 (Cambridge university press, 2003).
- [2] Grigory V Osipov, Jürgen Kurths, and Changsong Zhou, *Synchronization in oscillatory networks* (Springer Science & Business Media, 2007).
- [3] Susanna C Manrubia, Alexander S Mikhailov, *et al.*, *Emergence of dynamical order: synchronization phenomena in complex systems*, Vol. 2 (World Scientific, 2004).
- [4] Stefano Boccaletti, *The synchronized dynamics of complex systems*, Vol. 6 (Elsevier, 2008).
- [5] Andrzej Stefański, *Determining Thresholds of Complete Synchronization and Application*, Vol. 67 (World Scientific, 2009).
- [6] Takashi Nishikawa, ed., *Synchronization and Cascading Processes in Complex Networks [Focus Issue]*, Vol. 21 (AIP Publishing, 2011).
- [7] Johan AK Suykens and Grigory V Osipov, *Synchronization in complex networks [Focus Issue]*, Vol. 18 (AIP Publishing, 2008).
- [8] Juergen Kurths, Stefano Boccaletti, Celso Grebogi, and Ying-Cheng Lai, eds., *Control and synchronization in chaotic dynamical systems [Focus Issue]*, Vol. 13 (AIP Publishing, 2003).
- [9] Frank C Hoppensteadt and Eugene M Izhikevich, *Weakly connected neural networks*, Vol. 126 (Springer Science & Business Media, 2012).
- [10] John J Hopfield, “Neural networks and phys-

- ical systems with emergent collective computational abilities,” Proceedings of the National Academy of Sciences **79**, 2554–2558 (1982), <http://www.pnas.org/content/79/8/2554.full.pdf>.
- [11] Juan A. Acebrón, Luis L. Bonilla, Conrad J. Pérez Vicente, Félix Ritort, and Renato Spigler, “The kuramoto model: A simple paradigm for synchronization phenomena,” *Rev. Mod. Phys.* **77**, 137–185 (2005).
- [12] Toru Aonishi, “Phase transitions of an oscillator neural network with a standard hebb learning rule,” *Physical Review E* **58**, 4865 (1998).
- [13] Toshio Aoyagi and Katsunori Kitano, “Effect of random synaptic dilution in oscillator neural networks,” *Physical Review E* **55**, 7424 (1997).
- [14] Alex Arenas and Conrad J Pérez Vicente, “Exact long-time behavior of a network of phase oscillators under random fields,” *Physical review E* **50**, 949 (1994).
- [15] Frank C. Hoppensteadt and Eugene M. Izhikevich, “Oscillatory neurocomputers with dynamic connectivity,” *Phys. Rev. Lett.* **82**, 2983–2986 (1999).
- [16] Robert W Hölzel and Katharina Krischer, “Pattern recognition with simple oscillating circuits,” *New Journal of Physics* **13**, 073031 (2011).
- [17] Kathrin Kistorz, Robert W Hölzel, and Katharina Krischer, “Distributed coupling complexity in a weakly coupled oscillatory network with associative properties,” *New Journal of Physics* **15**, 083010 (2013).
- [18] Takashi Nishikawa, Frank C Hoppensteadt, and Ying-Cheng Lai, “Oscillatory associative memory network with perfect retrieval,” *Physica D: Nonlinear Phenomena* **197**, 134–148 (2004).
- [19] Rosangela Follmann, Elbert EN Macau, Epaminondas Rosa, and Jose RC Piqueira, “Phase oscillatory network and visual pattern recognition,” *Neural Networks and Learning Systems, IEEE Transactions on* **26**, 1539–1544 (2015).
- [20] Donald Olding Hebb, *The organization of behavior: A neuropsychological theory* (Psychology Press, 2005).
- [21] Robert W. Hölzel and Katharina Krischer, “Stability and long term behavior of a hebbian network of kuramoto oscillators,” *SIAM Journal on Applied Dynamical Systems* **14**, 188–201 (2015), <http://dx.doi.org/10.1137/140965168>.
- [22] Note that coupling modulations were named “coupling functions” by Hölzel [16], but this term is already used differently in the field.
- [23] Yoshiki Kuramoto, *Chemical oscillations, waves, and turbulence*, Vol. 19 (Springer Science & Business Media, 2012).
- [24] Toru Aonishi, Koji Kurata, and Masato Okada, “Acceleration effect of coupled oscillator systems,” *Phys. Rev. E* **65**, 046223 (2002).
- [25] Ferdinand Verhulst, *Nonlinear Differential Equations and Dynamical Systems*, Hochschultext / Universitext (Springer Berlin Heidelberg, 1996).
- [26] Solomon W Golomb, “The use of combinatorial structures in communication signal design,” in *Applications of Combinatorial Mathematics*, Institute of Mathematics and its Applications Conference Series, Vol. 60 (1997) pp. 59–78.
- [27] Mike D Atkinson and Anne-Lise Hassenklover, “Sets of integers with distinct differences,” in *Rep. SCS-TR-63* (School of Comp. Sci., Carleton Univ Ottawa, Ont., Canada, 1984).
- [28] Gyorgy Csaba and Wolfgang Porod, “Computational study of spin-torque oscillator interactions for non-boolean computing applications,” *Magnetics, IEEE Transactions on* **49**, 4447–4451 (2013).
- [29] Thomas C Jackson, Abhishek A Sharma, James A Bain, Jeffrey A Weldon, and Lawrence Pileggi, “Oscillatory neural networks based on tmo nano-oscillators and multi-level rram cells,” *Emerging and Selected Topics in Circuits and Systems, IEEE Journal on* **5**, 230–241 (2015).